# Exocytotic Fusion Pores are Composed of both Lipids and Proteins

Huan Bao[1,2], Marcel Goldschen-Ohm[1], Pia Jeggle[3], Baron Chanda[1], J. Michael Edwardson[3] and Edwin R. Chapman[1,2†]

[1]Department of Neuroscience, University of Wisconsin-Madison, 1111 Highland Ave., Madison, WI, 53705

[2]Howard Hughes Medical Institute, 1111 Highland Ave., Madison, WI, 53705

[3] Department of Pharmacology, University of Cambridge, Cambridge, UK

[†]Corresponding author: E-mail: chapman@wisc.edu

## Summary (138)

During exocytosis, fusion pores form the first aqueous connection that allows escape of neurotransmitters and hormones from secretory vesicles. Although it is well established that SNARE proteins catalyze fusion, the structure and composition of fusion pores remain unknown. Here, we employed the rigid framework and defined size of nanodiscs to interrogate the properties of reconstituted fusion pores, using the neurotransmitter glutamate as a content mixing marker. Efficient $Ca^{2+}$-stimulated bilayer fusion, and glutamate release, occurred with ~2 molecules of mouse synaptobrevin 2 reconstituted into ~6-nm nanodiscs. The transmembrane domains of SNARE proteins played distinct roles in lipid mixing versus content release, and were exposed to polar solvent during fusion. Also, tryptophan substitutions at specific positions in these transmembrane domains decreased glutamate flux. Together, these findings indicate that the fusion pore is a hybrid structure, composed of both lipids and proteins.

## Introduction

Membrane fusion and fission reactions underlie the compartmentalization that is a hallmark of all eukaryotic cells. Fusion underlies many processes ranging from fertilization and viral entry, to hormone signaling and synaptic transmission[1,2]. Defects in membrane fusion pathways are detrimental to cellular homeostasis, and are associated

with numerous human diseases[3-5]. In most cases, intracellular fusion reactions are directly mediated by soluble *N*-ethylmaleimide sensitive factor attachment protein receptors (SNAREs), which form the core of a conserved membrane fusion machine. In presynaptic nerve terminals, the SNARE complex that mediates synaptic vesicle (SV) exocytosis is composed of the vesicular SNARE (v-SNARE) synaptobrevin 2 (syb2; also referred to as VAMP2) , and the target membrane SNAREs (t-SNAREs) syntaxin 1A and SNAP-25B. These proteins assemble into four helix bundles with SNAP-25B contributing two helices, while syb2 and syx1A contribute one helix each[6]. v- and t-SNAREs have been proposed to progressively zipper from their N-terminal domains (NTDs) toward their C-terminal domains (CTDs), pulling the bilayers together and providing sufficient energy for fusion. SNARE complex assembly is strictly regulated by a large number of regulatory factors[7], including the $Ca^{2+}$ sensor for rapid neuronal exocytosis, synaptotagmin 1 (syt1)[8-10].

While the central role of SNAREs in membrane fusion is well established, the structure of the fusion pore remains enigmatic. Two distinct hypotheses have been proposed[11-13]. In the lipid-stalk-fusion hypothesis, the outer leaflets of the membranes destined to fuse first merge, forming a hemifusion stalk that resolves to a hemifusion diaphragm; the fusion pore then forms in the diaphragm, and is purely lipidic[14]. This model is supported by molecular dynamic simulations, and by physical chemistry experiments showing that membrane fusion, under specific conditions, can occur in the absence of proteins[15-18]. Alternatively, a proteinaceous fusion pore model has also been proposed, in which the fusion pore is lined by the transmembrane (TMDs) domains of syntaxin1A and synaptobrevin 2[11]. This model is supported by the findings that mutations in the transmembrane domains of SNARE proteins alter the flux of hormones through fusion pores in a predictable manner[19-21].

A major limitation in the study of fusion pores concerns their ephemeral nature. For example, in endocrine cells, the duration of the initial open state of the fusion pore is of the order of msec; the pore then either closes (kiss-and-run exocytosis) or dilates, resulting in full fusion[11,22]. The transient nature of fusion pores has severely limited biochemical efforts to probe their composition and structure. Here, we attempt to address

this critical question using the rigid framework of nanodiscs, which prevent the dilation of fusion pores. We developed an assay in which nanodiscs, bearing v-SNAREs, fused with small unilamellar vesicles that harbored t-SNAREs, in a manner that was accelerated by $Ca^{2+}$ and the $Ca^{2+}$ sensor for neuronal exocytosis, synaptotagmin-1. We also made use of a bona fide neurotransmitter, glutamate, to monitor flux through the reconstituted pores via an optical sensor, iGluSnFR[23]. We found that efficient $Ca^{2+}$-stimulated bilayer fusion, and glutamate release, required only two molecules of synaptobrevin 2 (syb2), and occurred using 6-nm nanodiscs. In addition, we show that the transmembrane domains of SNAREs are exposed to solvent during fusion. Collectively, these data reveal that the fusion pore is formed by a combination of lipids and SNARE transmembrane domains.

## Results

### Reconstitution of Syb2 into 6- and 13-nm Nanodiscs

According to the lipid-stalk-fusion hypothesis, the fusion pore is purely lipidic. Considering that each bilayer has a thickness of 4-5 nm[24,25], the fusion pore formed in nanodiscs will require a diameter >8 nm (Fig. 1a). Importantly, the size of nanodiscs can be controlled by the use of different membrane scaffold proteins (MSPs)[26]. In principle, the lipid-stalk-fusion model can be tested by using discs that are too small to allow for the formation of a purely lipidic pore. If pores are solely lipidic, they will not form between liposomes and 6-nm nanodiscs, whereas robust membrane fusion and content release should be observed using 13-nm nanodiscs. We note that an earlier study reported bilayer fusion, and content release, using SNAREs alone and 13-nm nanodiscs[27].

To conduct these experiments, syb2 was reconstituted into nanodiscs using MSP1D1ΔH4-H6 (to yield 6-nm discs)[28] and MSPE3D1 (to yield 13-nm discs)[26]. Size exclusion chromatography (SEC) analysis of these nanodiscs (Nd-V) revealed sizes of 90 ± 10 and 230 ± 20 kDa (Fig. 1b), respectively, using these two distinct scaffolding proteins. Taking into account of the size of the empty 6- and 13-nm nanodiscs (Supplementary Fig. 1a), we estimated that three and four molecules of syb2 were reconstituted into the small and large discs, respectively (we return to this point further below). Using atomic force

microscopy (AFM) imaging, the nanodisc diameters were determined to be 7.4 and 14 nm (Fig. 1c, d and Supplementary Fig. 1b), respectively; moreover, the size distributions were tightly clustered. Since scanning AFM imaging tends to overestimate the sizes of particles[29], and because the scaffolding proteins contribute to the measured diameter, the bilayer diameter in the small discs is likely to be 6 nm or less, consistent with previous studies[26,28]. In addition, we also reconstituted t-SNARE heterodimers into nanodiscs (Supplementary Fig. 1c, d). However, since SEC analysis revealed a broad elution profile indicative of a polydisperse sample, these discs were not used in the following experiments; rather, we focused on v-SNARE-bearing nanodiscs (Nd-V).

**Bilayer Fusion between Nanodiscs and Proteoliposomes**

We first used a lipid-mixing assay to test whether 6-nm and 13-nm nanodiscs can fuse with t-SNARE SUVs (Fig. 2 and Supplementary Fig. 2a). Nanodiscs were reconstituted with syb2, nitro-2-1,3-benzoxadiazol-4-yl-phosphatidylethanolamine (NBD-PE) and rhodamine-PE (1.5 mol% each); these probes are widely used to study SNARE-catalyzed fusion[8,27,30,31]. In this system, fusion between Nd-V and t-SNARE liposomes results in the dilution of NBD/rhodamine FRET pair and consequent dequenching of the NBD fluorescence, as we observed using both 6- and 13-nm nanodiscs (Fig. 2a,b). In the presence of the cytoplasmic domain of syt1 (comprising tandem $Ca^{2+}$-binding C2-domains tethered together by a short linker; designated C2AB), fusion was inhibited; then, upon addition of $Ca^{2+}$, fusion was strongly stimulated. Lipid mixing was not observed using protein-free (pf) liposomes or empty nanodiscs, and was blocked by addition of the cytoplasmic domain of syb2 (cd-v) or the cytoplasmic domain of t-SNAREs (cd-t) (Fig. 2e), demonstrating that lipid mixing was mediated by *trans*-SNARE pairing.

Since lipid mixing can be the result of hemi-fusion, rather than full fusion between nanodiscs and liposomes, we used dithionite to determine whether both leaflets fused in the nanodisc-SUV fusion assays[8,27]; lipid mixing in both leaflets is indicative of full fusion. We added dithionite, which irreversibly quenches the fluorescence of NBD, to samples after the initiation of lipid mixing. Since dithionite does not readily cross lipid bilayers, the

NBD in the inner-leaflet will be protected if: 1) full fusion occurred, and 2) fusion pores did not remain open after full fusion (Supplementary Fig. 2a). We note that a previous study reported that all fusion pores formed between nanodiscs and SUVs close, likely because of the extreme curvature of the fusion product[27]. Compared with detergent solubilized samples, protection from dithionite quenching, after fusion, is clearly observed using both 6-nm and 13-nm nanodiscs (Fig. 2c,d). Co-flotation assays and AFM imaging revealed that nanodiscs remained bound to t-SNARE liposomes (Supplementary Fig. 2d,e). Therefore, full fusion occurred, followed by closure of fusion pores via a mechanism that does not involve dissociation of the v-SNARE-bearing nanodiscs. Protection of NBD from dithionite was not observed using empty nanodiscs (Supplementary Fig. 2b), or when dithionite was added at the beginning of the reactions (Supplementary Fig. 2c), as the latter allows the reducing agent to enter the lumen of SUVs via nascent pores.

**Reconstitution of Glutamate Release Using Nanodiscs**

The fusion pore formed in nanodiscs can reseal and thus might not remain open long enough for neurotransmitter release, at least under some experimental conditions[27]. To address this, we tested whether a bona fide neurotransmitter, glutamate, can be released through fusion pores formed in the nanodisc-SUV fusion assay. Glutamate was encapsulated into t-SNARE liposomes, which were then incubated with Nd-V in the presence of an optical sensor for glutamate (iGluSnFR)[23]. Glutamate flux through the fusion pore results in a robust increase in the iGluSnFR fluorescence signal (Fig. 3a); this was observed using both 6- and 13-nm Nd-V (Fig. 3b,c), where release was strongly stimulated by adding C2AB plus $Ca^{2+}$. We also measured glutamate release using a wide range of nanodisc concentrations (Supplementary Fig.3). The data revealed a Hill coefficient of ~0.9, indicating that multiple nanodiscs do not work together, or cooperate, to destabilize vesicles and cause glutamate release. We conclude that $Ca^{2+}$-stimulated bilayer fusion and glutamate release can be reconstituted using 6-nm nanodiscs. Finally, we confirmed the findings obtained using C2AB by also reconstituting full-length syt1, and similar results were obtained (Supplementary Fig. 4).

Previous studies have shown that membrane fusion can be accompanied by the leak

of content mixing markers[32,33], so we set out to determine whether the $Ca^{2+}$-stimulated release of glutamate was indeed through fusion pores, or whether there is substantial leak. To address this, we turned to SUV-SUV fusion assays and took advantage of the glutamate-iGluSnFR reporter system. By placing the sensor in the media, outside of the liposomes, leak can be readily measured. This approach sharply contrasts the common use of self-quenching soluble fluorescent dyes as content release markers, as these reporters do not discriminate between flux through pores (from the lumen of one SUV to another) and leak (diffusion into the media).

t-SNARE liposomes, containing glutamate, were incubated with syb2 liposomes in the presence of $Ca^{2+}$ and C2AB (Fig. 3d). Glutamate leak during fusion between t- and v-SNARE liposomes was readily monitored via iGluSnFR in the media. We observed that high levels of syb2 (~1600 syb2/vesicle), in conjunction with a high concentration of $Ca^{2+}$-C2AB (10 μM), led to the excessive leak of glutamate (~70%). However, when low levels of syb2 (~ 80 syb2/vesicle) and $Ca^{2+}$-C2AB (1 μM) were used, glutamate leak was only ~5% (Fig. 3e). Hence, we utilized 1 μM C2AB, and always used $\leq$8 copies of syb2 per disc, in the following nanodisc-SUV fusion experiments, to ensure <5% glutamate leak. Since glutamate release in the nanodisc-SUV system is ~65-70%, neurotransmitter flux in this system mainly occurs through fusion pores; we return to this point further below, using mutant and modified SNAREs.

**Uncoupling Lipid Mixing from Content Mixing**

In the next series of experiments, we took advantage of the nanodisc-SUV fusion system to clarify whether alterations in SNARE proteins can differentially affect lipid mixing versus content release. We perturbed the TMD of syb2, and the SNARE motif of both syb2 and SNAP-25B (Fig. 4a), and studied how these alterations affected lipid mixing, cargo leak, and cargo flux (Fig. 4b-d).

Previous studies proposed that SNARE proteins progressively zipper together, in discrete stages, to form four helix bundles[34]. Thus, we used proline mutations, which perturb helices and often break helical continuity[35,36], to disrupt the SNARE motif in specific positions. Thus, proline substitutions were introduced in the second half of the

motif within syb2, at positions 60, 67, 74 and 81 (Fig. 4a). All of these mutants gave rise to similar levels of membrane leak (Fig. 4c), but yielded surprising effects on glutamate release and lipid mixing activity (Fig. 4b,d). The 60, 67, and 74P mutations resulted in modest, but significant and equal, reductions in lipid mixing activity. These same mutations had larger effects on glutamate release but, again, all three mutants appeared to be equivalent. However, a proline at position 81 profoundly inhibited content release as compared to lipid mixing activity. These experiments demonstrate that mutations in SNAREs can uncouple their function in lipid mixing versus content release, and that the extreme C-terminal end of the SNARE motif plays a particularly important role in content release[37], perhaps by holding the fusion pore open for a long enough time to allow efficient escape of cargo. These findings are further supported by the observation that deletion of layers 5-7 (Δlayer 5-7) in SNAP-25B had no effect on membrane leak, and only a modest effect on lipid mixing, but strongly inhibited glutamate flux through the pore. Again, the membrane proximal region of the SNARE motif appears to be particularly important for content release.

Next, the cytoplasmic domain of syb2 was fused to the cysteine-rich segment of the SV protein CSP (cysteine string protein), and the fusion protein was anchored onto the head-group of phosphatidyl ethanolamine (PE) on the nanodisc surface, through a maleimide-thiol reaction. The resulting mutant (designated syb-CSP) yielded 30% of the lipid mixing, and 10% of the glutamate release activity, exhibited by the wt protein (Fig. 4b,d). These results suggest that the TMD of syb2 might also have distinct functions during lipid mixing versus glutamate release. We explored this issue further by preparing a set of syb2 mutants that harbored truncations in their TMDs. Stepwise truncations from residue 116 to 108 of syb2 gradually decreased glutamate release, yet had no effect on lipid mixing[38]. In contrast, further truncation, by only two additional residues (to position 106) diminished both lipid mixing and glutamate release by 50% (Fig. 4b,d). Analogous to the proline mutations detailed above, membrane leak was not significantly affected by these deletions in the SNARE TMDs. In summary, the integrity of the syb2 TMD appears to play a key role in opening the fusion pore[39], or keeping it open, to yield efficient glutamate release, but is less important for lipid mixing.

**Two Molecules of Syb2 are Sufffient for $Ca^{2+}$-stimulated Fusion**

Six-nm nanodiscs are too small to accommodate the two lipid bilayers (each 4-5 nm thick) needed to form a purely lipidic fusion pore, yet membrane fusion and content release were observed. These findings suggest that the fusion pore might not proceed through the classical lipid-stalk-fusion model formed by only phospholipids[14]. We therefore conducted experiments to determine whether the pore is formed, in part, by the transmembrane domains of SNARE proteins, as posited by the proteinaceous fusion pore model[11]. To address this issue, we reconstituted increasing copy numbers of syb2 into nanodiscs, and determined the impact of copy number on bilayer fusion and glutamate release (Fig. 5). Nanodiscs (13 nm) containing 1 (ND1) to 8 (ND8) molecules of syb2 were generated (Supplementary Fig. 5a); the copy number was confirmed using size-exclusion chromatography (Fig. 5a) and single-molecule photobleaching experiments (Fig. 5d,e and Supplementary Fig. 5e-h).

In the absence of $Ca^{2+}$-C2AB, glutamate release fell from 70% to 5%, when the copy number of syb2 per nanodisc was reduced from eight to one (Fig. 5c). However, the lipid mixing signal decreased by ~ 50% (Fig. 5b). These results are consistent with a previous study, showing that content mixing, but not lipid mixing, is highly sensitive to the number of the SNARE complexes in the absence of additional regulatory proteins[27].

In contrast, in the presence of $Ca^{2+}$-C2AB, varying the number of syb2 molecules per nanodisc resulted in similar relative changes in both lipid mixing and glutamate release levels (Fig. 5b,c). Optimal fusion was achieved using nanodiscs containing three-to-four molecules of syb2. As shown previously, high copy numbers of syb2 resulted in inhibition by $Ca^{2+}$-C2AB[31], perhaps by interfering with the ability of $Ca^{2+}$-C2AB to bind to the membrane surface. A key finding was that two molecules of syb2 resulted in relatively efficient lipid mixing and glutamate release (~40% each; maximal efficiency was ~70%). Since single-molecule photobleaching experiments reveal that 99% of Nd2 nanodiscs contain only one-to-two molecules of syb2, fusion observed using Nd2 is not the result of a subpopulation of nanodiscs (<1%) that harbor more than two copies of syb2 (Fig. 5e). In line with this conclusion, we also prepared 6-nm nanodiscs that contained 2 molecules

of syb2 and, again, efficient lipid mixing and glutamate release was observed (Supplementary Fig. 5b-d). Since two molecules of syb2 are too few to form a proteinaceous channel, we posit that the fusion pore reconstituted in the nanodisc-SUV system is composed of both lipids and SNAREs. However, direct experiments, showing that the TMDs of SNAREs physically line the pore are needed to confirm this conclusion; these experiments are described below.

**TMDs of SNAREs Line the Fusion Pore**

If the fusion pore consists of both lipids and SNAREs, the SNARE TMDs should be transiently accessible to the media when the fusion pore opens. To test this hypothesis, we performed scanning cysteine accessibility assays on the TMDs of both syntaxin1A and syb2 (Fig. 6d-f). We initially attempted these experiments using cells. However, because of the short open lifetime of fusion pores, in conjunction with the fact that minute number of SNAREs are involved in fusion at any given time, these experiments were not successful. We therefore turned to the nanodisc-SUV system, as fusion pores cannot dilate, and efficient fusion is observed using a relatively low copy number of SNARE proteins.

MTSES, a membrane impermeant thiol-reactive probe, was used to probe for the exposure of single-cys residues - substituted in the TMDs of SNAREs - to the aqueous media when nanodiscs fuse with SUVs. These experiments revealed that specific residues within these TMDs are in fact labeled in a fusion-dependent manner (Fig. 6e,f); only low levels of labeling were observed in control experiments lacking a fusion partner (i.e. in the absence of nanodiscs or t-SNARE liposomes; also, labeling was not observed using protein free liposomes [data not shown]). Hence, the TMDs of SNARE are present within fusion pores and are transiently exposed to the media during fusion. In the crystal structure of the *cis*-SNARE complex, all the TMDs form $\alpha$–helices that coalesce into four-helix bundles[40]. When mapped onto these structures, the MTSES-labeled residues are all located on the same side of the syx1A and syb2 TMDs (Fig. 6g,h), so this face of the helix lines the pore.

To further corroborate this observation, we carried out Trp scanning mutagenesis of

the TMDs (Fig. 6a-c). As described in cell-based work, the bulky side-chains of Trp residues can, in principle, decrease transmitter flux by partially occluding a partially or completely proteinaceous fusion pore[19-21]. Under the conditions used, WT SNAREs, as well as most of the Trp mutants, gave rise to glutamate release efficiencies of ~ 65-75%. However, when specific residues were changed to Trp, a significant ($P < 0.05$ by two-tailed student's t-test; n = 5 technical repeats) further decrease of up to ~20% was observed (Fig. 6b,c). Four of these positions (271 and 279 of syx1A, 101 and 105 of syb2) correlated with the MTSES labeling experiments, corroborating the conclusion that these residues line the fusion pore during exocytosis. Two additional positions (269 and 283 in syx1A), when changed to Trp, also gave rise to diminished flux of glutamate but did not exhibit fusion-dependent MTSES labeling. There are a number of plausible explanations for this latter observation, including the possibility that these two Trp mutations shortened the fusion pore open time such that it could not be labeled chemically. Nonetheless, these experiments directly demonstrate that the TMDs of SNAREs physically line, in part, the nascent fusion pore.

**Discussion**

While progress has been made regarding the identification and reconstitution of the machinery that mediates neuronal exocytosis, the structure and composition of the central intermediate structure in the process - the fusion pore – remains unknown. This lack of information largely stems from the transient nature of fusion pore, which remains open for msec in neuroendocrine cells, and probably even a shorter time during SV exocytosis, before it rapidly dilates to yield full fusion, or closes again. Here, we took advantage of the rigid framework of nanodiscs, which prevent fusion pore dilation, in conjunction with biochemical approaches, to address the composition of reconstituted fusion pores. Our results are difficult to reconcile with either purely lipidic, or purely proteinaceous, fusion pores; rather, our findings indicate that the pore is lined by a combination of lipids and the TMDs of SNARE proteins.

Since each lipid bilayer is 4-5 nm thick, a 1 nm-wide fusion pore will require a nanodisc bilayer that is at least 9 nm diameter, according to the purely lipidic fusion pore

model. Consequently, we initially thought that fusion would not occur between 6-nm nanodiscs and liposomes. Surprisingly, our results show that $Ca^{2+}$-stimulated bilayer fusion, and glutamate release, can be reconstituted using 6-nm nanodiscs, suggesting that the fusion pore might not be formed via the simple merger of two lipid bilayers. The lipid mixing signals reported here do not arise from lipid transfer between the proximal leaflets (hemifusion), because dithionite quenching experiments demonstrate that lipid mixing occurred in both the outer and inner leaflets; the bilayers indeed fused in this system. We note that previous studies showed that placing additional amino acids at the C-terminus of the TMD of syb2 significantly decreases catecholamine release from cultured chromaffin cells[41], and that mutations in the TMDs of syx1A and syb2 alter hormone flux through fusion pores in PC12 cells and chromaffin cells, respectively[19-21]. These findings are also consistent with the idea that SNARE TMDs line the exocytotic fusion pore.

To monitor the release of a fluid phase marker from pores formed in the nanodisc-SUV system, we used a new approach based on glutamate, a bona fide neurotransmitter, in conjunction with the fluorescent glutamate sensor iGluSnFR[23]. In a previous study, high concentrations of $Ca^{2+}$ were used as the content marker[27], but high [$Ca^{2+}$] can directly affect the fusion of lipid bilayers[42,43], and can confound experiments that include the $Ca^{2+}$ sensor, syt1. Glutamate is an ideal cargo, as the flux of this transmitter mimics the release of glutamate from presynaptic boutons, without concerns about possible effects on the physical chemistry of the reconstituted membranes utilized in these *in vitro* studies. This approach will also facilitate comparisons between cell-based experiments with reconstitution approaches. However, one concern regarding the use of content release markers is the observation that membrane fusion can be accompanied by membrane leak, as shown during the fusion of yeast vacuoles[32]. At present, this caveat has not been carefully examined in reconstituted v-SUV/t-SUV fusion studies because the readout in previous studies was usually the dequenching of soluble fluorescent dyes upon dilution[44]; these reporters did not distinguish between membrane fusion and membrane leak. Using the glutamate-iGluSnFR reporter system, it was possible to determine the relationship between bilayer fusion, glutamate release, and

membrane leak during v-SUV and t-SUV fusion. We found that the extent of leak depends on the concentration of syb2 and C2AB; at a low copy number of syb2, and at low [C2AB], only low levels of membrane leak were observed (5%) (Fig. 3e), so these conditions were used for most of the experiments reported here. In addition, we found that membrane leak was not affected by proline mutations that disrupt full zippering of the SNARE motif or by deletions in the syb2 TMD (Fig. 4). So, leak can be readily uncoupled from flux through pores.

The data reported here indicate that the TMDs of SNAREs affect the dynamics of fusion pores by either increasing the probability of opening, or by increasing the open lifetime of pores to allow more efficient escape of content. This latter possibility could arise if a few residues in the TMDs of syb2 and syx 1A, near the interface of the membranes destined to fuse, physically interact with each other to hold pores open longer[40]. It should also be noted that SNAREs might oligomerize[45-47], and at high copy numbers could potentially form largely, or purely, proteinaceous channels[11-13]. Transient fusion pores, formed by the reversible assembly of SNAREs into oligomers, is an appealing idea as different stoichiometries of SNAREs might determine the size of the pore, which can range from 0.5 nm for small vesicles in the posterior pituitary to 2 nm in beige mouse mast cells[48,49]. In this light, we note that the number of SNAREs estimated to drive fusion range from two to fifteen in different kinds of cells[50-53].

We also observed that relatively efficient (~40%) glutamate release was achieved using only two copies of syb2, in the presence of $Ca^{2+}$-C2AB, supporting previous optical experiments showing that two copies of syb2 are sufficient for $Ca^{2+}$-triggered SV exocytosis from cultured neurons[50]. Since a proteinaceous channel requires at least three transmembrane domains, the fusion pore, reconstituted using two molecules of syb2, is likely to be composed of both lipids and SNARE TMDs. In summary, purely proteinaceous channels can, in principle, form at high copy numbers of SNAREs, but at low copy numbers, the fusion pore is composed of both lipids and proteins.

To determine directly whether SNARE TMDs transiently line fusion pores, and to probe their conformation during fusion, we performed scanning cysteine accessibility experiments, which revealed that residues in the TMDs are in fact exposed to solvent.

These findings provide the most direct support to date for the idea that SNARE TMDs comprise at least part of the fusion pore. Furthermore, systematic mutagenesis revealed positions in SNARE TMDs that, when substituted with bulky Trp residues, resulted in decreases in glutamate release. Similar Trp scanning experiments, carried out using secretory cells, also revealed reductions in hormone flux when the same residues, 101 and 105 in syb2, were mutated[21]. In the case of syx1A, our scanning Trp data (i.e. mutations at positions 271, 275 and 279 reduced flux) differed somewhat from the cell-based findings (mutations at positions 269, 276 and 283 reduced flux)[19]. This discrepancy might be due to different stoichiometries of SNAREs in cells versus our reconstituted system, as alluded to above. Future experiments, in which glutamate flux is measured at the single event level, are now required to address these issues.

**Acknowledgments:** We thank Gerhard Wagner for providing the MSPΔ1D1H4-H6 plasmid. This study was supported by a grant from the US National Institutes of Health (MH061876). H.B. is supported by a postdoctoral fellowship from Human Frontier Science Program. B.C. and M.P.G are supported by funding from the US National Institutes of Health (R01 GM084140). P.J. is supported by Kidney Research UK. J.M.E. is supported by the Biotechnology and Biological Sciences Research Council (BB/J018236/1) and Kidney Research UK. E.R.C. is supported as an Investigator of the Howard Hughes Medical Institute.

**Author Contribution**

M.G. and B.C. performed the single-molecule experiments; P.J. and J.M.E carried out the AFM experiments. H.B. performed nanodisc reconstitutions, fusion assays, and Cysteine accessibility assays; H.B. and E.C. conceived the project and designed the experiments. H.B. and E.C. wrote the paper and all other authors edited the manuscript.

**References**

1. Wickner, W. & Schekman, R. Membrane fusion. *Nat. Struct. Mol. Biol.* **15**, 658-64 (2008).
2. Rothman, J.E. The principle of membrane fusion in the cell (Nobel lecture). *Angew. Chem.*

*Int. Ed. Engl.* **53**, 12676-94 (2014).

3. Bolger, A.P. et al. Neurohormonal activation and the chronic heart failure syndrome in adults with congenital heart disease. *Circulation* **106**, 92-9 (2002).
4. Todde, V., Veenhuis, M. & van der Klei, I.J. Autophagy: principles and significance in health and disease. *Biochim. Biophys. Acta* **1792**, 3-13 (2009).
5. Westermann, B. Mitochondrial fusion and fission in cell life and death. *Nat. Rev. Mol. Cell Biol.***11**, 872-84 (2010).
6. Sutton, R.B., Fasshauer, D., Jahn, R. & Brunger, A.T. Crystal structure of a SNARE complex involved in synaptic exocytosis at 2.4 A resolution. *Nature* **395**, 347-53 (1998).
7. Jahn, R. & Fasshauer, D. Molecular machines governing exocytosis of synaptic vesicles. *Nature* **490**, 201-7 (2012).
8. Bhalla, A., Chicka, M.C., Tucker, W.C. & Chapman, E.R. Ca2+-synaptotagmin directly regulates t-SNARE function during reconstituted membrane fusion. *Nat. Struct. Mol. Biol.* **13**, 323-330 (2006).
9. Chicka, M.C., Hui, E., Liu, H. & Chapman, E.R. Synaptotagmin arrests the SNARE complex before triggering fast, efficient membrane fusion in response to Ca2+. *Nat. Struct. Mol. Biol.* **15**, 827-35 (2008).
10. Lai, Y. et al. Fusion pore formation and expansion induced by Ca2+ and synaptotagmin 1. *Proc. Natl. Acad. Sci. USA* **110**, 1333-8 (2013).
11. Jackson, M.B. & Chapman, E.R. The fusion pores of Ca2+ -triggered exocytosis. *Nat. Struct. Mol. Biol.* **15**, 684-9 (2008).
12. Lindau, M. & Almers, W. Structure and function of fusion pores in exocytosis and ectoplasmic membrane fusion. *Curr. Opin. Cell Biol.* **7**, 509-17 (1995).
13. Fang, Q.H. & Lindau, M. How Could SNARE Proteins Open a Fusion Pore? *Physiology* **29**, 278-285 (2014).
14. Chernomordik, L.V. & Kozlov, M.M. Mechanics of membrane fusion. *Nat. Struct. Mol. Biol.* **15**, 675-83 (2008).
15. Kozlovsky, Y. & Kozlov, M.M. Stalk model of membrane fusion: Solution of energy crisis. *Biophys. J.* **82**, 882-895 (2002).
16. Weinreb, G. & Lentz, B.R. Analysis of membrane fusion as a two-state sequential process:

Evaluation of the stalk model. *Biophys. J.* **92**, 4012-4029 (2007).

17. Chakraborty, H., Tarafdar, P.K., Bruno, M.J., Sengupta, T. & Lentz, B.R. Activation Thermodynamics of Poly(Ethylene Glycol)-Mediated Model Membrane Fusion Support Mechanistic Models of Stalk and Pore Formation. *Biophys. J.* **102**, 2751-2760 (2012).
18. Chernomordik, L.V., Melikyan, G.B. & Chizmadzhev, Y.A. Biomembrane Fusion - a New Concept Derived from Model Studies Using 2 Interacting Planar Lipid Bilayers. *Biochim. Biophys. Acta* **906**, 309-352 (1987).
19. Han, X., Wang, C.T., Bai, J., Chapman, E.R. & Jackson, M.B. Transmembrane segments of syntaxin line the fusion pore of Ca2+-triggered exocytosis. *Science* **304**, 289-92 (2004).
20. Han, X. & Jackson, M.B. Electrostatic interactions between the syntaxin membrane anchor and neurotransmitter passing through the fusion pore. *Biophys. J.* **88**, L20-L22 (2005).
21. Chang, C.W. et al. A Structural Role for the Synaptobrevin 2 Transmembrane Domain in Dense-Core Vesicle Fusion Pores. *J. Neurosci.* **35**, 5772-5780 (2015).
22. Alabi, A.A. & Tsien, R.W. Perspectives on Kiss-and-Run: Role in Exocytosis, Endocytosis, and Neurotransmission. *Annu. Rev. Physiol.* **75**, 393-422 (2013).
23. Marvin, J.S. et al. An optimized fluorescent probe for visualizing glutamate neurotransmission. *Nat. Methods* **10**, 162-170 (2013).
24. Hristova, K. & White, S.H. Determination of the hydrocarbon core structure of fluid dioleoylphosphocholine (DOPC) bilayers by x-ray diffraction using specific bromination of the double-bonds: effect of hydration. *Biophys. J.* **74**, 2419-33 (1998).
25. Lewis, B.A. & Engelman, D.M. Lipid bilayer thickness varies linearly with acyl chain length in fluid phosphatidylcholine vesicles. *J. Mol. Biol.* **166**, 211-7 (1983).
26. Denisov, I.G., Grinkova, Y.V., Lazarides, A.A. & Sligar, S.G. Directed self-assembly of monodisperse phospholipid bilayer nanodiscs with controlled size. *J. Am. Chem. Soc.* **126**, 3477-3487 (2004).
27. Shi, L. et al. SNARE Proteins: One to Fuse and Three to Keep the Nascent Fusion Pore Open. *Science* **335**, 1355-1359 (2012).
28. Hagn, F., Etzkorn, M., Raschle, T. & Wagner, G. Optimized Phospholipid Bilayer Nanodiscs Facilitate High-Resolution Structure Determination of Membrane Proteins. *J.*

*Am. Chem. Soc.* **135**, 1919-1925 (2013).

29. Sun, S. et al. Receptor binding enables botulinum neurotoxin B to sense low pH for translocation channel assembly. *Cell Host Microbe.* **10**, 237-47 (2011).
30. Weber, T. et al. SNAREpins: minimal machinery for membrane fusion. *Cell* **92**, 759-72 (1998).
31. Tucker, W.C., Weber, T. & Chapman, E.R. Reconstitution of Ca2+-regulated membrane fusion by synaptotagmin and SNAREs. *Science* **304**, 435-8 (2004).
32. Starai, V.J., Jun, Y. & Wickner, W. Excess vacuolar SNAREs drive lysis and Rab bypass fusion. *Proc. Natl. Acad. Sci. USA* **104**, 13551-8 (2007).
33. Nickel, W. et al. Content mixing and membrane integrity during membrane fusion driven by pairing of isolated v-SNAREs and t-SNAREs. *Proc. Natl. Acad. Sci. USA* **96**, 12571-6 (1999).
34. Gao, Y. et al. Single reconstituted neuronal SNARE complexes zipper in three distinct stages. *Science* **337**, 1340-3 (2012).
35. Senes, A., Engel, D.E. & DeGrado, W.F. Folding of helical membrane proteins: the role of polar, GxxxG-like and proline motifs. *Curr. Opin. Struct. Biol.***14**, 465-79 (2004).
36. McNew, J.A. et al. Close is not enough: SNARE-dependent membrane fusion requires an active mechanism that transduces force to membrane anchors. *J. Cell Biol.* **150**, 105-17 (2000).
37. Sorensen, J.B. et al. Sequential N- to C-terminal SNARE complex assembly drives priming and fusion of secretory vesicles. *EMBO J* **25**, 955-66 (2006).
38. Xu, Y., Zhang, F., Su, Z., McNew, J.A. & Shin, Y.K. Hemifusion in SNARE-mediated membrane fusion. *Nat. Struct. Mol. Biol.* **12**, 417-22 (2005).
39. Grote, E., Baba, M., Ohsumi, Y. & Novick, P.J. Geranylgeranylated SNAREs are dominant inhibitors of membrane fusion. *J. Cell Biol.* **151**, 453-66 (2000).
40. Stein, A., Weber, G., Wahl, M.C. & Jahn, R. Helical extension of the neuronal SNARE complex into the membrane. *Nature* **460**, 525-U105 (2009).
41. Ngatchou, A.N. et al. Role of the synaptobrevin C terminus in fusion pore formation. *Proc. Natl. Acad. Sci. USA* **107**, 18463-8 (2010).
42. Kachar, B., Fuller, N. & Rand, R.P. Morphological responses to calcium-induced

interaction of phosphatidylserine-containing vesicles. *Biophys. J.* **50**, 779-88 (1986).

43. Hui, S.W., Nir, S., Stewart, T.P., Boni, L.T. & Huang, S.K. Kinetic measurements of fusion of phosphatidylserine-containing vesicles by electron microscopy and fluorometry. *Biochim. Biophys. Acta* **941**, 130-40 (1988).
44. Ma, C., Su, L., Seven, A.B., Xu, Y. & Rizo, J. Reconstitution of the vital functions of Munc18 and Munc13 in neurotransmitter release. *Science* **339**, 421-5 (2013).
45. Hohl, T.M. et al. Arrangement of subunits in 20 S particles consisting of NSF, SNAPs, and SNARE complexes. *Mol. Cell* **2**, 539-548 (1998).
46. Rickman, C., Hu, K., Carroll, J. & Davletov, B. Self-assembly of SNARE fusion proteins into star-shaped oligomers. *Biochem. J.* **388**, 75-9 (2005).
47. Roy, R., Laage, R. & Langosch, D. Synaptobrevin transmembrane domain dimerization-revisited. *Biochemistry* **43**, 4964-70 (2004).
48. Klyachko, V.A. & Jackson, M.B. Capacitance steps and fusion pores of small and large-dense-core vesicles in nerve terminals. *Nature* **418**, 89-92 (2002).
49. Breckenridge, L.J. & Almers, W. Final steps in exocytosis observed in a cell with giant secretory granules. *Proc. Natl. Acad. Sci. USA* **84**, 1945-9 (1987).
50. Sinha, R., Ahmed, S., Jahn, R. & Klingauf, J. Two synaptobrevin molecules are sufficient for vesicle fusion in central nervous system synapses. *Proc. Natl. Acad. Sci. USA* **108**, 14318-23 (2011).
51. Hua, Y. & Scheller, R.H. Three SNARE complexes cooperate to mediate membrane fusion. *Proc. Natl. Acad. Sci. USA* **98**, 8065-70 (2001).
52. Mohrmann, R., de Wit, H., Verhage, M., Neher, E. & Sorensen, J.B. Fast Vesicle Fusion in Living Cells Requires at Least Three SNARE Complexes. *Science* **330**, 502-505 (2010).
53. Montecucco, C., Schiavo, G. & Pantano, S. SNARE complexes and neuroexocytosis: how many, how close? *Trends Biochem. Sci.***30**, 367-372 (2005).

## Figure legends

### Figure 1. Reconstitution of syb2 into 6-and 13-nm Nanodiscs.

(a) Illustration of a lipidic fusion pore, and the relative sizes of the two kinds of nanodiscs employed in this study. (b) Size-exclusion chromatography of 6- and 13-nm nanodiscs. (c-d) Diameter distributions of 6- (d) and 13-nm nanodiscs (c) determined by AFM imaging. Data represent means ± s.d. (n = number of particles analyzed).

**Figure 2. Bilayer Fusion between v-SNARE Nanodiscs (Nd-V) and t-SNARE Vesicles.**

(a-b) Time courses of lipid mixing using 13- (a) and 6-nm (b) Nd-V, in the presence and absence of C2AB (with or without free $Ca^{2+}$) and cd-V. (c-d) Dithionite quenching after fusion between t-SNARE vesicles and 13- (c) or 6-nm (d) Nd-V. a.u.: arbitrary units. (e) Nd-SUV lipid mixing assays were performed using t-SNARE liposomes, pf-liposomes, or empty-nanodiscs; in each case assays were run in the presence and absence of cd-v, cd-t, and C2AB in the presence of 1 mM $Ca^{2+}$ (shown) or 0.2 mM EGTA (data not shown). Data represent means ± s.d. (n = 3 technical replicates).

**Figure 3. Reconstitution of Glutamate Release using Nanodiscs.**

(a) Illustration summarizing the glutamate release assay. During fusion between Nd-V and t-SNARE vesicles, glutamate is released through the fusion pore, resulting in increases in the fluorescence signal of the glutamate sensor (iGluSnFR). (b-c) Time courses of glutamate release using 13-nm (b) and 6-nm (c) Nd-V. (d) Illustration summarizing the membrane leak assay utilizing v- and t-SNARE vesicles. Glutamate leak, during fusion between v-SNARE and t-SNARE liposomes, was detected via iGluSnFR. (e) Glutamate leak as a function of [$Ca^{2+}$-C2AB] and v-SNARE copy number. Data represent means ± s.d. (n = 3 technical replicates).

**Figure 4. Distinct Structural Elements of SNAREs Differentially Affect Bilayer fusion, Membrane leak, and Glutamate release.**

(a) Illustration of the alterations in syb2 and SNAP-25B used to dissociate their functions in lipid mixing, content leak, and flux through fusion pores. Constructs: syb-CSP, the cytoplasmic domain of syb2 was fused to the cysteine-rich segment of the SV protein

CSP (cysteine string protein); Δlayer 5-7, deletion from layer 5 to 7 in the second SNARE motif of SNAP-25B; Δlayer 7, deletion of layer 7 in the same motif of SNAP-25B. (b-d) Characterization of SNARE mutants using glutamate release (b), glutamate leak (c) and lipid mixing assays (d). Data represent means ± s.d. (n = 3 technical replicates)

**Figure 5. Two Molecules of syb2 Mediate Efficient Membrane Fusion and Content Release.**

(a) Size-exclusion chromatography profiles of nanodiscs containing 1 to 8 molecules of syb2. (b-c) Lipid mixing (b) and glutamate release (c), measured in the absence and presence of $Ca^{2+}$-C2AB, are plotted versus the syb2 copy number per nanodisc. Data represent means ± s.d. (n = 3 technical replicates) (d) Examples of single molecule photobleaching traces. (e) Histograms of the number of observed photobleaching steps fit to either a Poisson distribution or a binomially weighted Poisson distribution. $< n >$ is the average number of syb2 molecules per nanodisc.

**Figure 6. SNARE TMDs are Present in the Fusion Pore.**

(a) Illustration of the scanning Trp assay. Glutamate release efficiency mediated by Trp mutant forms of syntaxin (b) and syb2 (c). Data represent means ± s.d. (n = 5 technical replicates). (d) Illustration of the substituted cysteine accessibility assay to probe the TMDs of syb2 and syx1A during fusion. The accessibility of single-Cys substitutions in syx1A (e) and syb2 (f), with (red trace) or without (black trace) fusion, as measured via the degree of MTSES labeling. Data represent means ± s.d. (n = 3 technical replicates). Solvent-exposed residues (red) are mapped onto the structure of syxtaxin (g) and syb2 (h).

## Online Methods

### Reagents

Nitrilotriacetic acid ($Ni^{2+}$-NTA)-chelating Sepharose and Superdex 200 were obtained from GE Healthcare. N-dodecylphosphocholine (DPC),

1-palmitoyl-2-oleoyl-*sn*-glycero-3-phosphocholine (PC),
1,2-dioleoyl-*sn*-glycero-3-phospho-l-serine (PS),
1-palmitoyl-2-oleoyl-*sn*-glycero-3-phosphoethanolamine (PE),
1,2-dioleoyl-*sn*-glycero-3-phospho-(1'-myo-inositol-4',5'-bisphosphate) ($PI(4,5)P_2$),
1,2-dioleoyl-*sn*-glycero-3-phosphoethanolamine-*N*-(biotinyl) (biotin-PE),
1,2-dipalmitoyl-*sn*-glycero-3-phospho-ethanolamine-*N*-(7-nitro-2-1,3-benzoxadiazol-4-yl) (NBD-PE) and *N*-(lissamine rhodamine B sulfonyl)-1,2-dipalmitoyl-*sn*-glycero-3-phosphoethanolamine (rhodamine-PE) were obtained from Avanti Polar Lipids. 2-Sulfonatoethyl methanethiosulfonate sodium salt (MTSES) was purchased from Biotium. All other chemicals were from Sigma.

**Recombinant Proteins**

Syb2 and t-SNARE heterodimers were purified as previously described[1,2], except that *n*-Dodecyl β-D-maltoside (DDM) and N-dodecylphosphocholine (DPC), respectively, were used in place of *n*-octyl glucoside (OG). Purification of full length (residues 1-421) and the cytoplasmic domain (C2AB; residues 96-421) of syt1 was carried out as described previously[3]. Purification of the glutamate sensor (iGluSnFR), and the membrane scaffold proteins (MSPE3D1 and MSPΔ1D1H4-H6), was carried out as described previously[4-6].

**Proteoliposome Reconstitution**

SNARE proteins were mixed together with lipids (15% PE, 25% PS and 60% PC) in reconstitution buffer (25 mM HEPES pH 7.5, 100 mM KCl, 1mM DTT) plus 0.02% DDM. To encapsulate glutamate into proteoliposomes, 50 mM glutamate was included in the mixture. For fusion assays involving full-length syt1, 2% $PI(4,5)P_2$ was included in the t-SNARE liposomes. Detergent was removed using BioBeads under gentle shaking (overnight, 4 °C). t-SNARE liposomes were then isolated by flotation[1], followed by dialysis against reconstitution buffer (overnight, 4 °C). Trypsin digestion experiments revealed that ~50-70% of SNARE proteins were correctly oriented (data not shown).

**Nanodisc Reconstitution**

Nanodisc reconstitution was performed as described[7,8]. A typical reconstitution experiment involved mixing together syb2, MSP and lipids (15% PE, 40% PS and 45% PC) in reconstitution buffer containing 0.02% DDM. To prepare nanodiscs for lipid mixing experiments, the lipid composition was: 12% PE, 40% PS, 45% PC, 1.5% NBD-PE and 1.5% rhodamine-PE. For 13-nm nanodiscs, the ratio of MSP:lipid was 2:120, whereas a ratio of 2:30 was used for 6-nm nanodiscs. To prepare nanodiscs containing different copy numbers of syb2, the following MSP:syb2 ratios were used: 2:0.2 (ND1), 2:0.4 (ND2), 2:1 (ND3), 2:2 (ND4), 2:4 (ND5), 2:6 (ND6), 2:8 (ND7) and 2:10 (ND8). Detergent was slowly removed using BioBeads (1/3 volume, Sigma) with gentle shaking (overnight, 4°C). The reconstituted discs were centrifuged (20 min at 100,000 × g) and purified with $Ni^{2+}$-NTA beads, followed by gel filtration using a Superdex 200 10/300 GL column equilibrated in reconstitution buffer plus 5% glycerol.

**Lipid Mixing Assay**

Lipid mixing assays were carried out as described[1,2], using nanodiscs (0.2 μM) and t-SNARE liposomes (0.5 μM) in the absence and presence of C2AB (1 μM). The reaction mixtures were incubated at 37 °C for 10 min in reconstitution buffer plus 0.2 mM EGTA, followed by addition of $Ca^{2+}$ (1 mM final concentration). The NBD signal was monitored for an additional 1 h. After each run, 20 μl 2.5 % of DDM was added to each reaction to calculate the maximal fluorescence signal and data were collected for another 25 min. The maximal fluorescence signal after addition of detergent, minus the fluorescence signal at the beginning of the assay, was used to normalize the % of lipid mixing. Data were obtained from three independent trials.

**Glutamate Release Assay**

Glutamate release assays were performed using the glutamate sensor iGluSnFR (1 μM)[6], nanodiscs (0.2 μM) and glutamate encapsulated t-SNARE liposomes (0.5 μM) in the absence and presence of C2AB (1 μM). The reaction mixtures were incubated at 37 °C for 20 min in reconstitution buffer plus 0.2 mM EGTA, followed by addition of $Ca^{2+}$ (1 mM final concentration), and the iGluSnFR fluorescence signal was monitored for

an additional 1 h. After each run, 20 µl 2.5 % of DDM was added to each reaction and data were collected for another 25 min. Data were obtained from three independent trials.

**Scanning Cysteine Accessibility Method**

Nd-V (0.2 µM) and t-SNARE liposomes (0.5 µM ) were incubated with MTSES (0.1 mM) at 37 °C for 1h, in the presence of $Ca^{2+}$ (1 mM) and $C2AB_{C277A}$ (0.1 µM). The reaction mixture was diluted 20-fold into 25 mM HEPES pH 7.5, plus 5 mM cysteine, followed by centrifugation at 150,000 × *g* at 4 °C for 40 min in a Beckman Optima MAX-E (Beckman Coulter) tabletop ultracentrifuge. The pellets were washed with 25 mM HEPES pH 7.5, and resuspended in labeling buffer (25 mM HEPES pH 7.5, 6M urea and 0.5% DDM); samples were then incubated with 5-Iodoacetamidofluorescein (5-IAF, 0.1 mM) at 37 °C for 1h and subjected to SDS-PAGE, followed by fluorescence scanning and Coomassie blue staining. MTSES labelling efficiency was determined by protection from 5-IAF labeling in comparison with controls that were not treated with MTSES. Data were obtained from three independent trials.

**AFM Imaging**

Purified v-SNARE nanodiscs and t-SNARE liposomes were suspended in HBS (100 mM NaCl, 50 mM HEPES, pH 7.5) containing 1 mM $CaCl_2$, and 45 µl of the sample was deposited onto freshly-cleaved mica (10 mm diameter discs). After a 5-min adsorption period, the sample was rinsed with the same buffer solution to remove unabsorbed material. AFM imaging was carried out using a Dimension FastScan Bio AFM. All samples were imaged in tapping mode (in fluid) using silicon nitride probes (FastScan D, Bruker AFM Probes). These cantilevers had a spring constant of ~0.25 N/m and a drive frequency of ~85 kHz (10–20% below the resonance frequency). The applied imaging force was kept as low as possible ($A_S/A_0$~0.85). Images were captured at a scan rate of 20 Hz, with 512 scan lines per area. Data analysis was performed using Gwyddion 2.40 software. Nanodisc diameter was determined by drawing cross-sections of the imaged structures.

**Single Molecule Photobleaching**

Syb2-61C/103A was incubated with Cy5 or DY650 maleimide at a molar ratio of 1:5 (room temperature, 3h). Labeled protein was purified using a Zeba$^{TM}$ desalting column (Life Technologies) equilibrated in reconstitution buffer containing 0.02% DDM. The labeling efficiency was ~ 0.6 and 0.7 for Cy5 and DY650, respectively. For single-molecule photobleaching experiments, the lipid composition for nanodiscs was: 1% biotin-PE, 14% PE, 40% PS and 45% PC. Purified nanodiscs containing syb2-DY650 were immobilized on a biotin/streptavidin-coated surface within arrays of zero-mode waveguide nanoholes (~200 nm diameter, Pacific Biosciences) and imaged on an inverted microscope (Olympus IX71) with a 100x oil immersion objective (Olympus, NA=1.49). Imaging buffer was 10 mM $Na_2HPO_4$ pH 7, 2 mM $KH_2PO_4$, 200 mM NaCl, 2 mg/ml BSA, 1 mM TCEP, 2.5 mM PCA, 250 nM PCD, and 1 mM Trolox. Concentrations of syb2-DY650 were chosen so that approximately 1% of the nanoholes in each imaged array contained fluorescent dye, such that each nanohole could be reasonably assumed to contain at most one nanodisc. DY650 was excited by epi-illumination from a 637 nm laser (Coherent OBIS). Each zero-mode waveguide nanohole limits the effective excitation volume to attoliters at the optical surface such that only fluorescence from surface-immobilized dye is observed. Fluorescence, from arrays of ~1000 nanoholes, was imaged using a 512x512 EMCCD camera (Andor iXon Ultra 9899) after passing through a dichroic and emission filter (Semrock Brightline FF560/659-Di01 and FF01-577/690, respectively).

Bleach step distributions were initially described by a Poisson distribution assuming that incorporation of syb2 molecules into nanodiscs was both random and independent.

$$Poisson(k,\lambda) = \frac{\lambda^k}{k!}e^{-\lambda}$$

where $k$ is the number of bleach steps and $\lambda$ is the average number of fluorescently labeled syb2 molecules per nanodisc. If each syb2 molecule has a probability $p < 1$ of having a fluorescent label, the observed number of bleach steps $k$ for nanodiscs containing $n$ syb2 molecules will be described by a Binomial distribution.

$$Binomial(k,n,p) = \binom{n}{k} p^k (1-p)^{n-k}$$

Thus, to account for incomplete fluorescent dye labeling of syb2, we further fitted bleach step distributions to a weighted Poisson distribution where the probability of observing $k$ bleach steps is given by

$$wPoisson(k,\lambda,p) = \sum_{n=k}^{N} Poisson(n,\lambda)\, Binomial(k,n,p)$$

where $\lambda$ is the average number of syb2 molecules per nanodisc (labeled or not), $p$ is the probability that each syb2 molecule has a fluorescent label, and $N$ is the maximum possible number of syb2 molecules per nanodisc (in practice any $N$ large enough such that $Poisson(N,\lambda)$ is negligible). The summation includes the probabilities that $k$ observed bleach steps came from $n \geq k$ molecules with fractional labeling $p$ weighted by the Poisson probability of having $n$ molecules.

## References for Online Method


1. Bhalla, A., Chicka, M.C., Tucker, W.C. & Chapman, E.R. Ca2+-synaptotagmin directly regulates t-SNARE function during reconstituted membrane fusion. *Nat. Struct. Mol. Biol.* **13**, 323-330 (2006).
2. Tucker, W.C., Weber, T. & Chapman, E.R. Reconstitution of Ca2+-regulated membrane fusion by synaptotagmin and SNAREs. *Science* **304**, 435-8 (2004).
3. Wang, Z., Liu, H., Gu, Y. & Chapman, E.R. Reconstituted synaptotagmin I mediates vesicle docking, priming, and fusion. *J. Cell. Biol.* **195**, 1159-70 (2011).
4. Denisov, I.G., Grinkova, Y.V., Lazarides, A.A. & Sligar, S.G. Directed self-assembly of monodisperse phospholipid bilayer nanodiscs with controlled size. *J. Am. Chem. Soc.* **126**, 3477-3487 (2004).
5. Hagn, F., Etzkorn, M., Raschle, T. & Wagner, G. Optimized Phospholipid Bilayer Nanodiscs Facilitate High-Resolution Structure Determination of Membrane Proteins. *J. Am. Chem. Soc.* **135**, 1919-1925 (2013).
6. Marvin, J.S. et al. An optimized fluorescent probe for visualizing glutamate

neurotransmission. *Nat. Methods* **10**, 162-170 (2013).

7. Shi, L. et al. Preparation and characterization of SNARE-containing nanodiscs and direct study of cargo release through fusion pores. *Nat. Protoc.* **8**, 935-948 (2013).
8. Shi, L. et al. SNARE Proteins: One to Fuse and Three to Keep the Nascent Fusion Pore Open. *Science* **335**, 1355-1359 (2012).

Figure 1

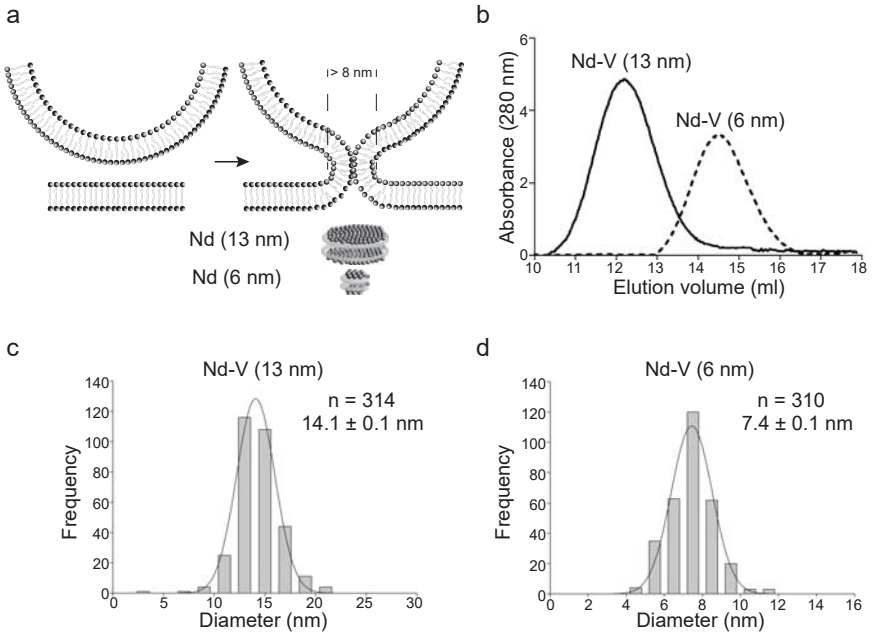
a
> 8 nm
Nd (13 nm)
Nd (6 nm)
b
Nd-V (13 nm)
Nd-V (6 nm)
Absorbance (280 nm)
Elution volume (ml)
c
Nd-V (13 nm)
n = 314
14.1 ± 0.1 nm
Frequency
Diameter (nm)
d
Nd-V (6 nm)
n = 310
7.4 ± 0.1 nm
Frequency
Diameter (nm)

Figure 2

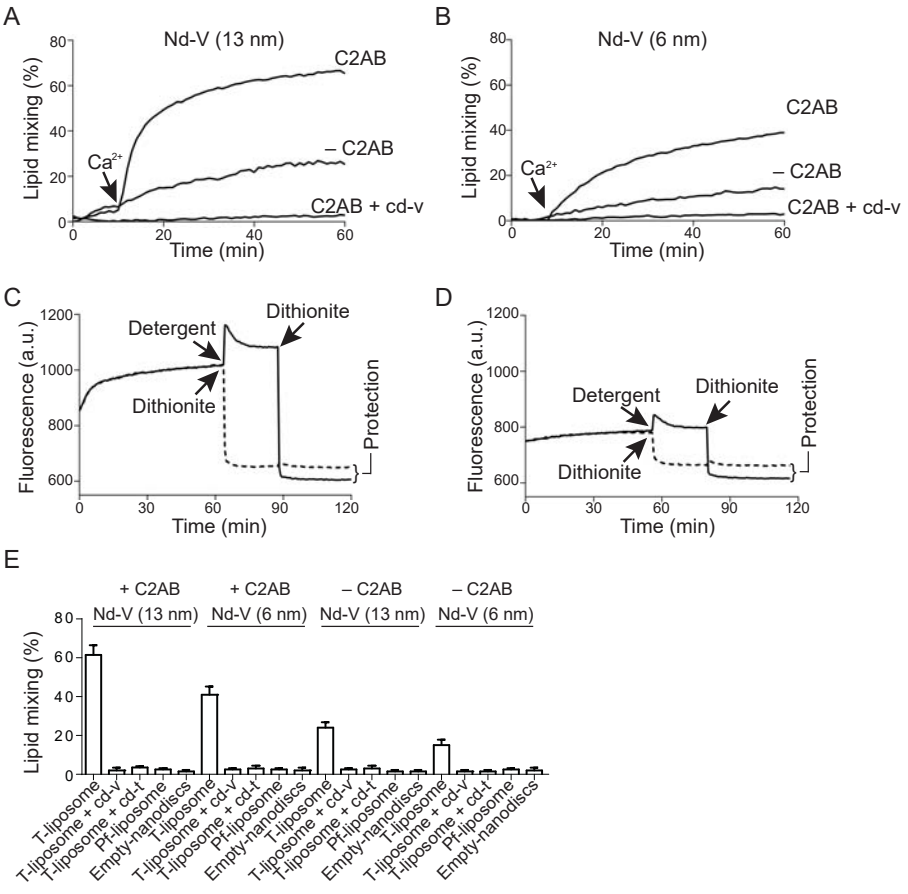
A
Nd-V (13 nm)
C2AB
– C2AB
C2AB + cd-v
Ca2+
Lipid mixing (%)
Time (min)
B
Nd-V (6 nm)
C2AB
– C2AB
C2AB + cd-v
Ca2+
Lipid mixing (%)
Time (min)
C
Detergent
Dithionite
Dithionite
Protection
Fluorescence (a.u.)
Time (min)
D
Detergent
Dithionite
Dithionite
Protection
Fluorescence (a.u.)
Time (min)
E
+ C2AB
+ C2AB
– C2AB
– C2AB
Nd-V (13 nm)
Nd-V (6 nm)
Nd-V (13 nm)
Nd-V (6 nm)
Lipid mixing (%)
T-liposome
T-liposome + cd-v
T-liposome + cd-t
Pf-liposome
Empty-nanodiscs

Figure 3

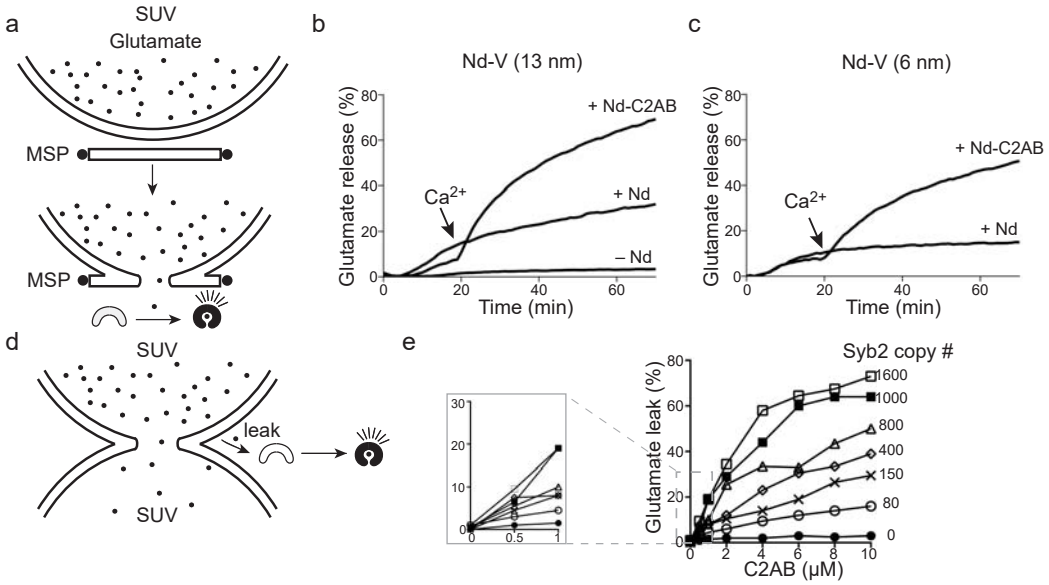
a
SUV
Glutamate
MSP
MSP
b
Nd-V (13 nm)
Glutamate release (%)
+ Nd-C2AB
+ Nd
– Nd
Ca2+
Time (min)
c
Nd-V (6 nm)
Glutamate release (%)
+ Nd-C2AB
+ Nd
Ca2+
Time (min)
d
SUV
leak
SUV
e
Syb2 copy #
1600
1000
800
400
150
80
0
Glutamate leak (%)
C2AB (μM)

Figure 4

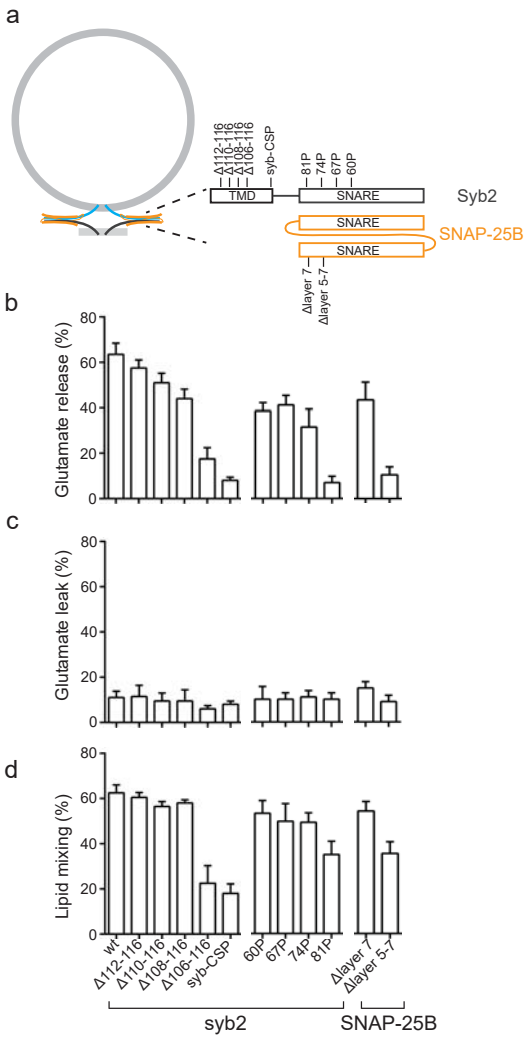
a
Δ112-116
Δ110-116
Δ108-116
Δ106-116
syb-CSP
81P
74P
67P
60P
TMD
SNARE
Syb2
SNARE
SNAP-25B
SNARE
Δlayer 7
Δlayer 5-7
b
Glutamate release (%)
0
20
40
60
80
c
Glutamate leak (%)
0
20
40
60
80
d
Lipid mixing (%)
0
20
40
60
80
wt
Δ112-116
Δ110-116
Δ108-116
Δ106-116
syb-CSP
60P
67P
74P
81P
Δlayer 7
Δlayer 5-7
syb2
SNAP-25B

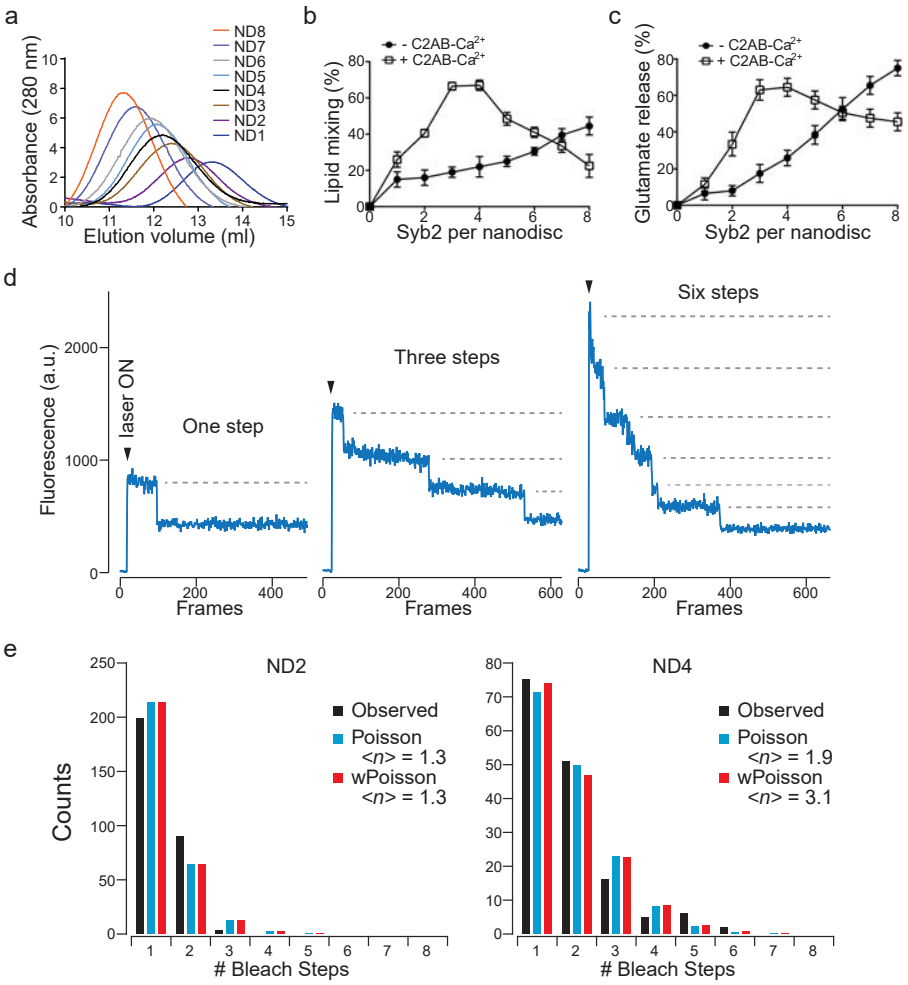
a
Absorbance (280 nm)
Elution volume (ml)
ND8
ND7
ND6
ND5
ND4
ND3
ND2
ND1
b
Lipid mixing (%)
- C2AB-Ca2+
+ C2AB-Ca2+
Syb2 per nanodisc
c
Glutamate release (%)
- C2AB-Ca2+
+ C2AB-Ca2+
Syb2 per nanodisc
d
Fluorescence (a.u.)
laser ON
One step
Three steps
Six steps
Frames
e
Counts
ND2
Observed
Poisson
<n> = 1.3
wPoisson
<n> = 1.3
# Bleach Steps
ND4
Observed
Poisson
<n> = 1.9
wPoisson
<n> = 3.1
# Bleach Steps

Figure 6

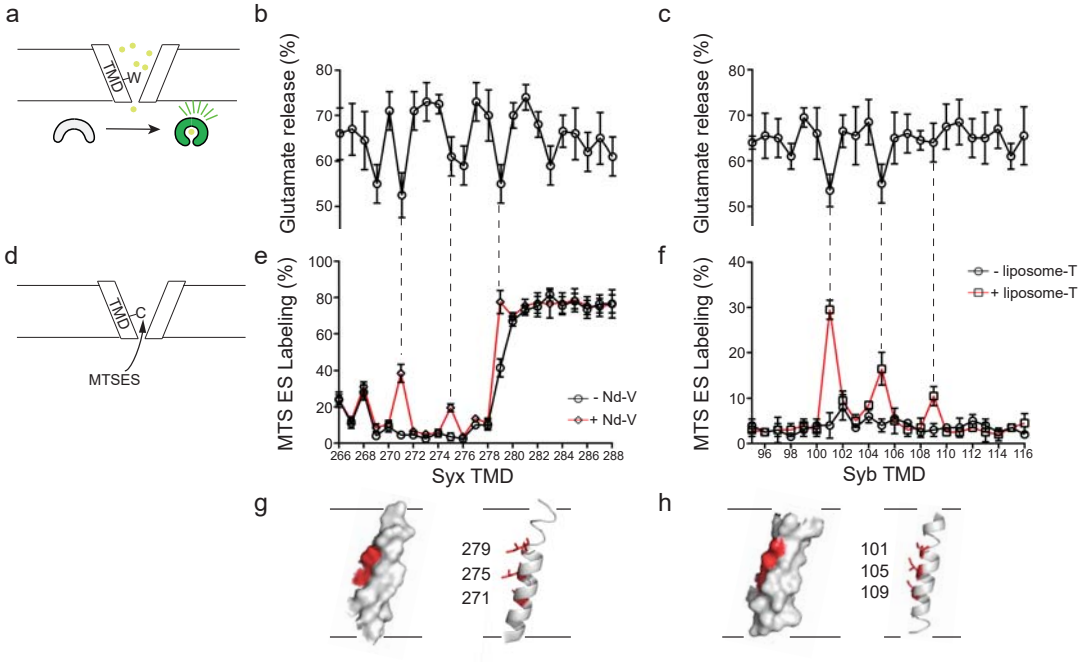
a
TMD
W
b
Glutamate release (%)
c
Glutamate release (%)
d
TMD
C
MTSES
e
MTS ES Labeling (%)
- Nd-V
+ Nd-V
Syx TMD
f
MTS ES Labeling (%)
- liposome-T
+ liposome-T
Syb TMD
g
279
275
271
h
101
105
109

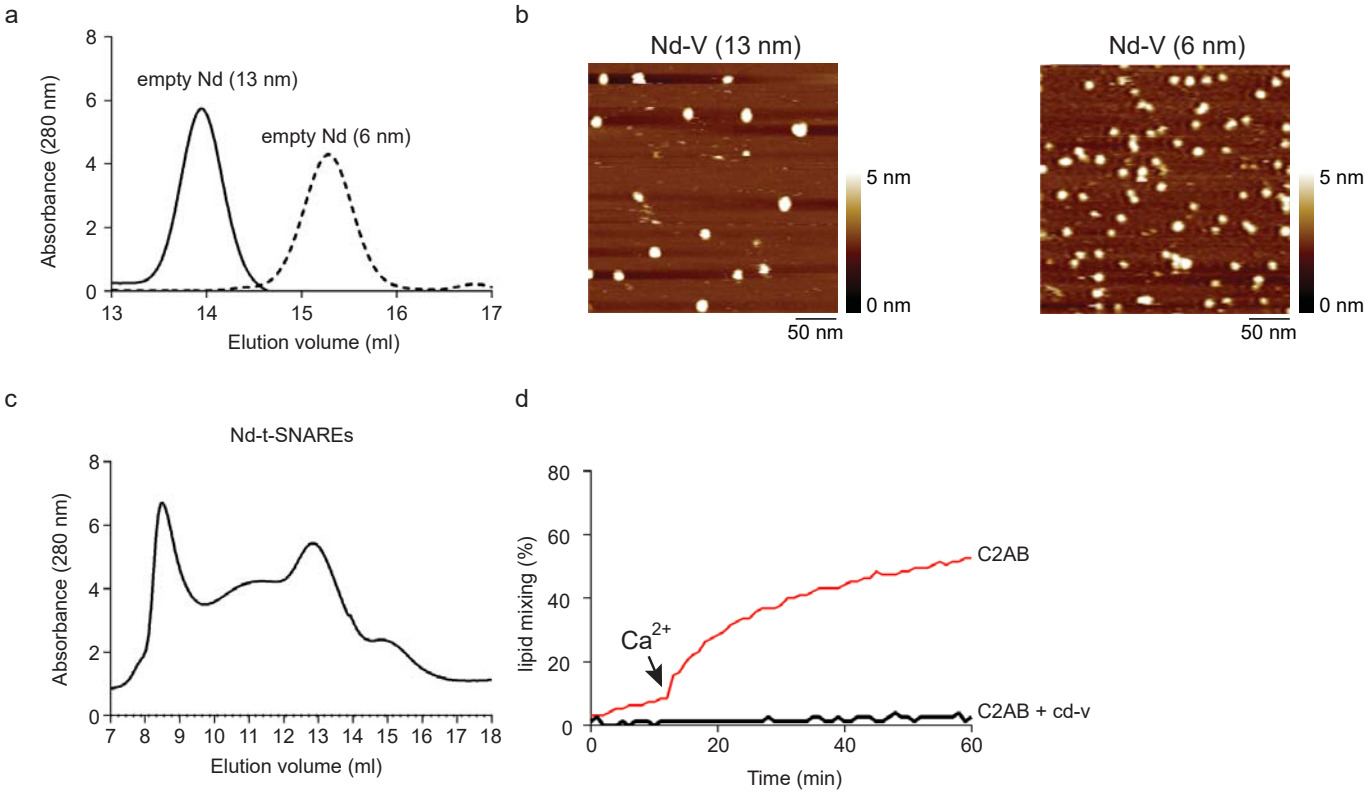


**Supplementary Figure 1. Characterization of Nanodiscs.**

(a) Empty nanodiscs were analyzed using a Superdex 200 10/300 GL column equilibrated in 25 mM HEPES pH 7.5, 100 mM KCl, 1mM DTT and 5% glycerol. (b) AFM images of v-SNARE nanodiscs. (c) t-SNARE nanodiscs were analyzed using a Superdex 200 10/300 column as described in *panel A*. (d) Lipid mixing between t-SNARE nanodiscs and v-SNARE vesicles was monitored in the presence of $Ca^{2+}$ (1 mM) and C2AB, with and without cd-v.

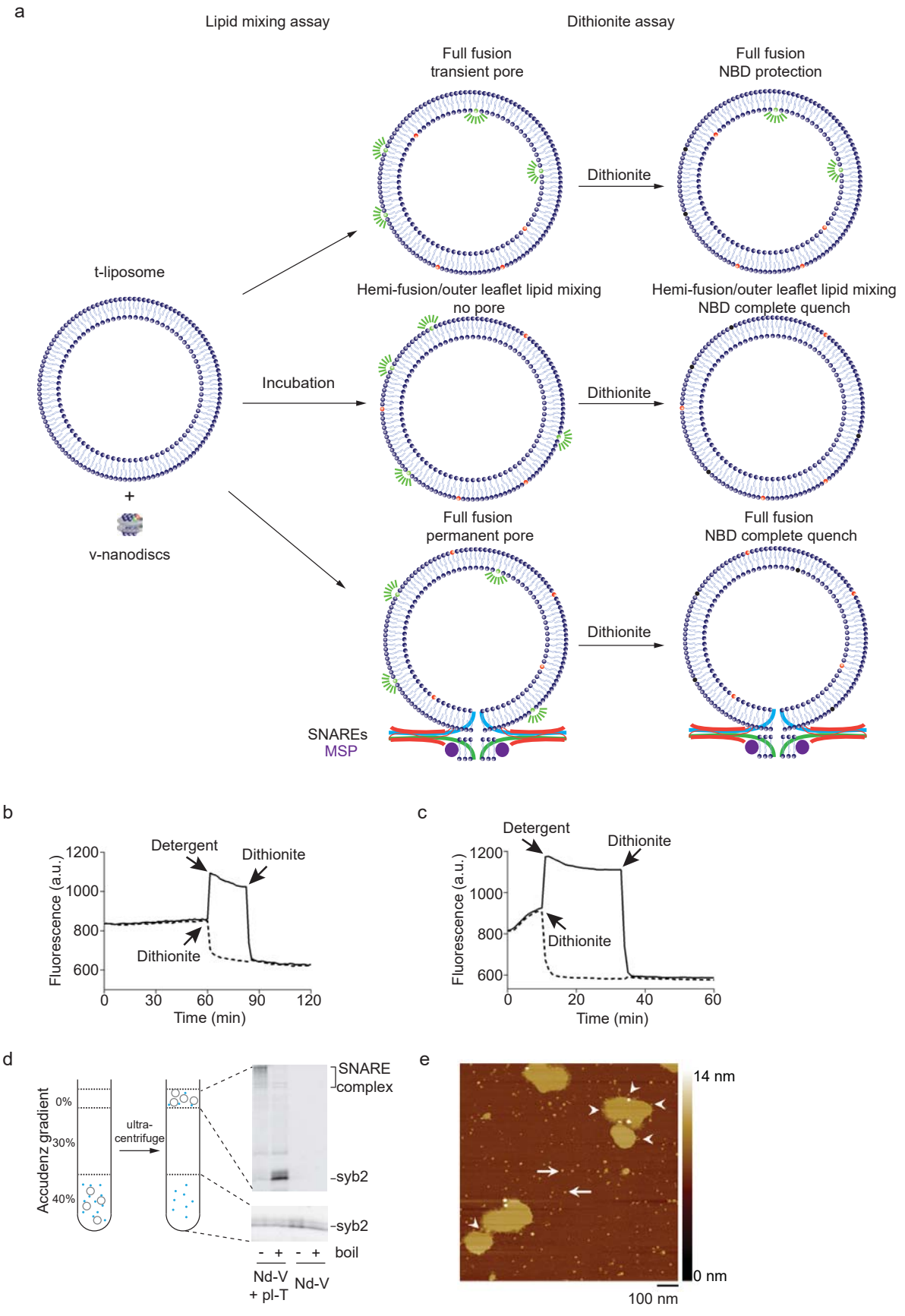
a
Lipid mixing assay
Dithionite assay
Full fusion
transient pore
Full fusion
NBD protection
Dithionite
t-liposome
Hemi-fusion/outer leaflet lipid mixing
no pore
Hemi-fusion/outer leaflet lipid mixing
NBD complete quench
Incubation
Dithionite
+
v-nanodiscs
Full fusion
permanent pore
Full fusion
NBD complete quench
Dithionite
SNAREs
MSP
b
Detergent
Dithionite
Dithionite
Fluorescence (a.u.)
1200
1000
800
600
0
30
60
90
120
Time (min)
c
Detergent
Dithionite
Dithionite
Fluorescence (a.u.)
1200
1000
800
600
0
20
40
60
Time (min)
d
Accudenz gradient
0%
30%
40%
ultra-
centrifuge
SNARE
complex
syb2
syb2
boil
- + - +
Nd-V
+ pl-T
Nd-V
e
14 nm
0 nm
100 nm

**Supplementary Figure 2. All Fusion Pores Close After Fusion.**

(a) Illustration of lipid mixing and dithionite quenching experiments. (b-c) Protection of NBD fluorescence is not observed using empty nanodiscs (b) or when dithionite is added at the beginning of the fusion reaction (c). (d) Left Panel: illustration of the co-flotation assay. Samples containing syb2 nanodiscs and t-SNARE liposomes were mixed with an equal volume of 80% Accudenz, and then layered with 30% and 0% Accudenze. Ultra-centrifugation was carried out at 55,000 rpm at 4 °C for 2 h. Samples were collected at the 40% Accudenze layer and at the 30%-0% interface. Right panel: DY650-labeled syb2 nanodiscs (Nd-V) were incubated with or without t-SNARE liposomes (pl-T) at 37 °C for 1 h in the presence of $Ca^{2+}$ (1 mM) and C2AB (1 μm). Samples were analyzed by co-flotation, and the top and bottom fractions were subjected to SDS-PAGE and fluorescence scanning. (e) Syb2 nanodiscs were incubated with t-SNARE liposomes at 37 °C for 1 h, followed by AFM analysis. Arrows indicate free nanodiscs; arrowheads indicate liposome-associated nanodiscs. Scale bar: 100 nm.

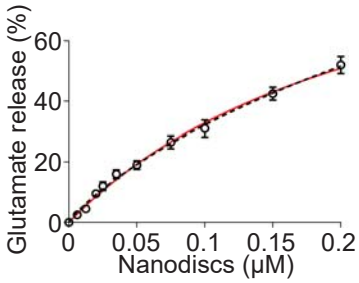


**Supplementary Figure 3. Glutamate release during SUV-nanodisc fusion as a function of 6-nm nanodisc concentration.**

Data were fitted to the Hill (black dotted line) and Michaelis-Menten equations (red line). Data points are presented as mean ± s.d. from three independent trials.

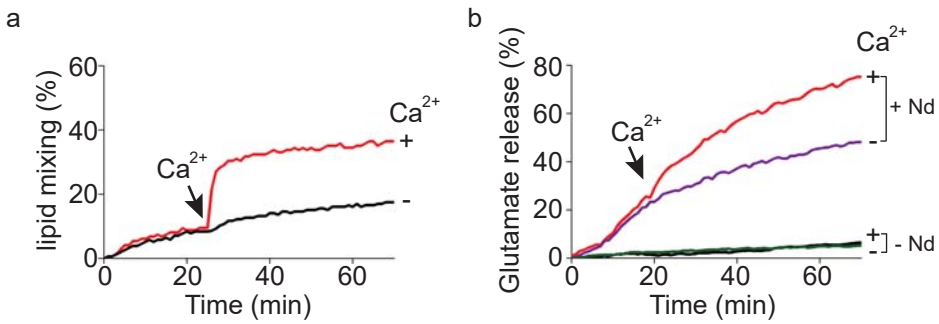


**Supplementary Figure 4. Reconstitution of $Ca^{2+}$-Triggered Lipid Mixing and Glutamate Release Using Full-length Syt1.**

(a) Lipid mixing between t-SNARE vesicles and nanodiscs harboring syb2 and full-length syt1. (b) Glutamate release from t-SNARE vesicles in the presence and absence of nanodiscs harboring syb2 and full-length syt1. Arrow indicates the addition of $Ca^{2+}$ (1 mM final concentration).

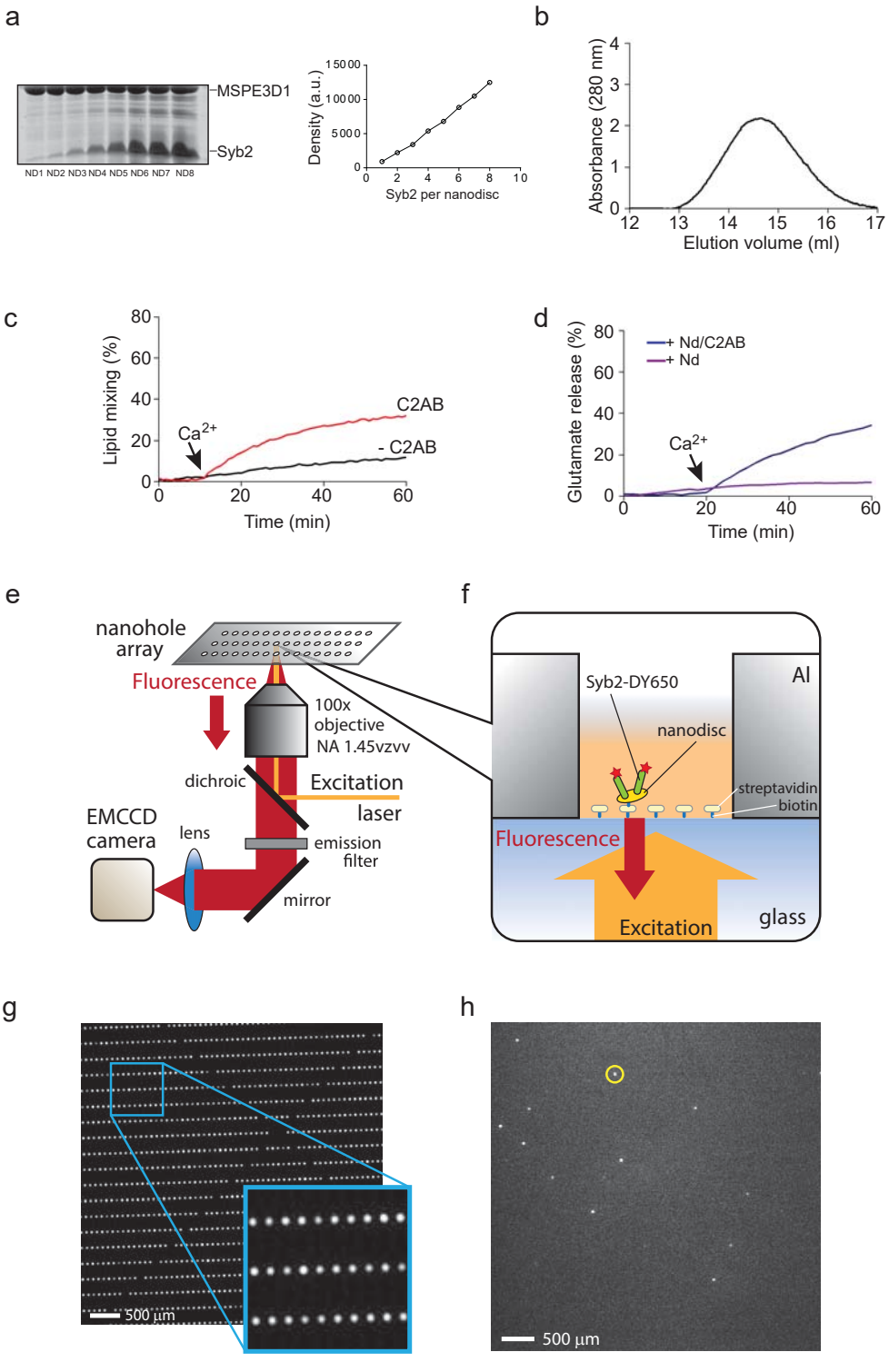
a
MSPE3D1
Syb2
ND1 ND2 ND3 ND4 ND5 ND6 ND7 ND8
Density (a.u.)
Syb2 per nanodisc
b
Absorbance (280 nm)
Elution volume (ml)
c
Lipid mixing (%)
Ca2+
C2AB
- C2AB
Time (min)
d
Glutamate release (%)
+ Nd/C2AB
+ Nd
Ca2+
Time (min)
e
nanohole array
Fluorescence
100x objective NA 1.45vzvv
dichroic
Excitation laser
EMCCD camera
lens
emission filter
mirror
f
Syb2-DY650
Al
nanodisc
streptavidin
biotin
Fluorescence
Excitation
glass
g
500 µm
h
500 µm

**Supplementary Figure 5**. **Efficient $Ca^{2+}$-Triggered Bilayer Fusion and Glutamate Release Occurs Using Two v-SNAREs in 6-nm Nanodiscs.**

(a) Left panel: SDS-PAGE of nanodiscs (ND1, ND2, ND3, ND4, ND5, ND6, ND7 and ND8). Right panel: densitometry of the syb2 protein bands from the gel in panel (a) were plotted versus the syb2 copy number per nanodisc. (b) Size exclusion chromatography of 6-nm ND2. (c) Lipid mixing between 6-nm ND2 and t-SNARE vesicles, in the presence and absence of C2AB; addition of $Ca^{2+}$ (1 mM final concentration) is indicated by an arrow. (d) Glutamate release from t-SNARE vesicles in the presence of 6-nm ND2 and C2AB; the arrow indicates the addition of $Ca^{2+}$ (1 mM final concentration). (e) Experimental setup for imaging bleaching steps from arrays of zero-mode waveguide nanoholes containing single nanodiscs that bear fluorescently labeled syb2. (f) Illustration of an individual zero-mode waveguide nanohole with a nanodisc containing two syb2-DY650 molecules immobilized on the glass surface via biotin/streptavidin. Fluorescence from DY650 was measured upon epi laser illumination, with the effective excitation volume limited to attoliters. (g) Brightfield image of an array of zero-mode waveguide nanoholes with diameters of ~ 200 nm. (h) Fluorescence image of an array as in (g) after sparse labeling with syb2-DY650 containing nanodiscs such that only a few nanoholes contained a single nanodisc (one of these is indicated with a yellow circle).